JOM, Vol. 71, No. 4, 2019
https://doi.org/10.1007/s11837-019-03382-2

Intrinsic Heat Treatment Within Additive Manufacturing of Gamma Titanium Aluminide Space Hardware

ANDRÉ SEIDEL,[1,4] SHUVRA SAHA,[1] TIM MAIWALD,[1,2] JULIANE MORITZ,[1] STEFAN POLENZ,[1] AXEL MARQUARDT,[1,2] JOERG KASPAR,[1] THOMAS FINASKE,[1] ELENA LOPEZ,[1] FRANK BRUECKNER,[1,3] and CHRISTOPH LEYENS[1,2]

1.—Fraunhofer-Institute for Material and Beam Technology, Winterbergstraße 28, 01277 Dresden, Germany. 2.—Technische Universität Dresden, Helmholtzstr. 7, 01069 Dresden, Germany. 3.—Luleå University of Technology, 971 87 Luleå, Sweden. 4.—e-mail: andre.seidel@iws.fraunhofer.de

A major part of laser additive manufacturing focuses on the fabrication of metallic parts for applications in the space and aerospace sectors. Especially, the processing of the very brittle titanium aluminides can be particularly challenging because of their distinct tendency to lamellar interface cracking. In the present paper, a gamma titanium aluminide (γ-TiAl) nozzle, manufactured via electron beam melting, is extended and adapted via hybrid laser metal deposition. The presented example considers a new field of application for this class of materials and approaches the process-specific manipulation of the composition and/or microstructure via the adjustment of processing temperatures, temperature gradients and solidification conditions. Furthermore, intrinsic heat treatment is investigated for electron beam melting and laser metal deposition with powder, and the resulting influence is releated to conventional processing.

INTRODUCTION

During the last three decades, intermetallics have been of enormous interest in material science and technology with respect to applications at high temperatures.[1] Within this period of time, a new class of materials was developed, and titanium aluminides, based on the ordered gamma titanium aluminide (γ-TiAl) phase, have found applications in the aircraft engine industry.[2,3] The advantages of this class of innovative high-temperature materials are their low density, in the range of 3.9–4.2 g cm^{-3}, good strength and creep properties up to 750°C as well as their good oxidation and burn resistance.[1,4] Examples for applications are the low-pressure turbine blades of the Pratt & Whitney geared turbofan^{TM} engine, PW1100G,[2] and the high-bypass turbofan engine, LEAP-1A, from GE Aviation Safran Aircraft Engines.[3] The present paper exemplarily addresses cold-gas propulsion systems. Due to their simplicity, cold-gas propulsion systems have the potential to provide orbital manoeuvrings capability for small, micro- and even nano-satellites.[5] The major benefits obtained from this system are the low budget, mass and volume. These systems mainly consist of a propellant tank, solenoid valves, thrusters, tubing and fittings.[6] Thrusters are the convergent–divergent nozzles that provide the desired amount of thrust to perform manoeuvres in space. The rather new concept of cold-gas propulsion systems uses propellants that enter the nozzle at elevated temperatures, resulting in significantly enhanced thrust and an increased specific impulse compared to conventional cold-gas flow.[7,8] In fact, the investigations of Gilpin et al.[9] indicate an increase of the specific impulse, a measure of how effectively a rocket uses propellant, from 60 s to more than 250 s if the temperature is raised to approximately 725°C. Hence, TiAl-based alloys may enable the improvement of the specific impulse and reduce weight in the same manner. Nevertheless, the interaction between the propellant, in the latter case ammonia, and TiAl-based alloys is still under investigation,[10] but there is rather a short time exposure because of the limited quantity of propellant that can be taken on board.[11–13] On the other

(Published online February 25, 2019)

hand, there are also noble gases like argon or helium widely used in cold-gas thrusters.[14] Either way, the segment of nano-/microsatellites shows a high double-digit growth since 2010, while each individual application leads to a unique set of requirements for the system.[5] In consequence, additive manufacturing is assumed as a manufacturing option which is faster, cheaper and less complex for thruster nozzles, adding the possibility to achieve a new freedom of design. In addition, there is the potential of customized thermal processing which can exploit a further degree of freedom in terms of microstructural tailoring; the latter, of course, in the long-term perspective after appropriate investigation and qualification.

GAMMA TITANIUM ALUMINIDE ALLOYS

TiAl alloys have a wide range of attractive properties such as high specific strength, good corrosion and oxidation resistance, high stiffness and creep resistance. The influencing factors behind these improved properties are, namely, alloying elements, processing techniques and subsequent heat treatments. Hence, TiAl alloys represent an interesting alternative to the usual CGT candidates, stainless steel, aluminium and titanium,[15] if the operating temperatures are in a temperature range of 550–750°C.[16] Then, however, the increase in performance goes along with weight reduction. Nevertheless, TNM alloys are focussed on in this paper. The acronym TNM has arisen from the first letter of the constituting alloying elements such as T stands for TiAl, N for Nb and M for Mo. TNM alloys represent β-solidified multi-phase γ-TiAl-based alloys with a nominal composition as shown into Table I.[17,18]

An important representative of this group of alloys is Ti-43.5Al-4Nb-1Mo-0.1B (at.%). The equilibrium diagram of this alloy undergoes the following phase transformation sequence:

$$L \rightarrow L+\beta \rightarrow \beta \rightarrow \beta+\alpha \rightarrow \beta+\alpha+\gamma \rightarrow \beta+\beta_0+\alpha+\gamma \rightarrow \beta_0+\alpha+\gamma \rightarrow \beta_0+\alpha+\alpha_2+\gamma \rightarrow \beta_0+\alpha_2+\gamma \quad (1)$$

Due to the addition of β-stabilizing elements like Nb and Mo, the eutectoid line is converted into a four-phase-field ($\beta_0 + \alpha + \alpha_2 + \gamma$), so two new eutectoid points have originated, which are defined as the starting and finishing temperatures.[18] Moreover, at the nominal composition, there is no chance of peritectic solidification or the formation of a single α-phase field which it is not actually desired, because of the extreme growth rate during post-processing heat treatment.[19] In the above composition, 0.1 at.% B was found to be an effective grain refiner; however, TiB2 precipitation is not considered in the transformation sequence.

Ti-borides work as an inoculant where heterogeneous nucleation of the β-phase field occurs during solid-state phase transformation (see Table II) according to Burger's orientation relationship.[20,21] Further cooling increases γ precipitation from the α/α_2 phase, followed by Blackburn orientation relationship, through the diffusion process, resulting in α/γ or $\alpha_2 + \gamma$ colonies.[22,23] Table II summarizes important transition temperatures relevant to the intrinsic heat treatment in additive processing (see Fig. 2) with reference to Fig. 1.

Another characteristic of these alloys is their brittle, ceramic-like behavior at room temperature and their ductile metallic behavior at elevated temperature. This change in behavior, called the brittle-to-ductile transition temperature (BDTT), usually ranges from 600°C to 820°C, depending on the chemical composition and microstructure of the alloy.[24] To reduce thermally-induced stresses and to avoid cracking, in this case lamellar interface cracking,[25–28] preheating is frequently applied.[29,30] For titanium aluminides, the pre-heating temperature is in commonly chosen significantly above BDTT in the range of 1000°C.[31–33] These process temperatures raise the issue of the high solubility of O_2 in Ti-alloys which can go up to 25 at.% which deteriorates the mechanical properties. An increasing Al content limits the oxygen inward diffusion because Al_2O_3 is formed as a barrier. At very high Al contents, a continuous, protective Al_2O_3-layer is formed on $TiAl_3$ during high-temperature oxidation and no oxygen is found underneath.[34] Nevertheless, there is also considerably improved oxidation

Table I. Constitution of the 3rd generation alloys TNMTM alloy family and impact of the alloying elements[17,18]

Alloying elements (at.%): Ti-(42-48)Al-(0-4)Cr,Mn,V-(0-10)Nb,Ta,W,Mo-(0-2)Si,C,B

Element	Phase	Impact
Al	α_2-Ti_3Al	High strength, low RT ductility and a low oxidation resistance
Cr, Mn, V	β/β_0	High RT ductility, superplasticity
Nb, Ta, W, Mo		Refinement of the microstructure, improvement of the hot-workability and oxidation resistance
Si, C, B	Silicides, carbides borides	Refinement of the microstructure, improvement of the creep strength

Table II. Phase transition temperature of TNM alloys close to its thermodynamic equilibrium

Alloy	Exp. composition (at.%)	T_{eu} (°C)	$T_{\gamma,solv}$ (°C)	$T_{\beta 0 \rightarrow \beta}$ (°C)	References
A	Ti-43.67Al-4.08Nb-1.02Mo-0.1B	1160	1255	1175–1205	Schwaighofer et al.[23]
B	Ti-43.3Al-4.3Nb-1.2Mo-0.1B	1175	1265	1195–1215	Erdely et al.[24]

T_{eu} eutectoid temperature, $T_{\gamma,solv}$ γ-solvus temperature, $T_{\beta 0 \rightarrow \beta}$ β-phase ordering temperature.

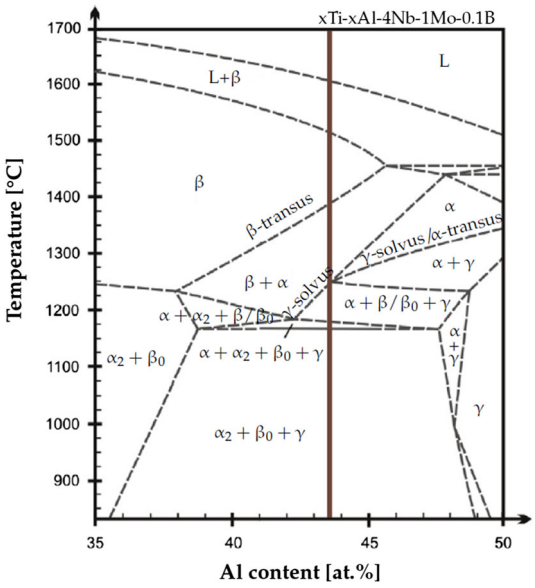

Fig. 1. Section of TNM alloy system of nominal composition Ti-43.5Al-4Nb-1Mo-0.1B.[18]

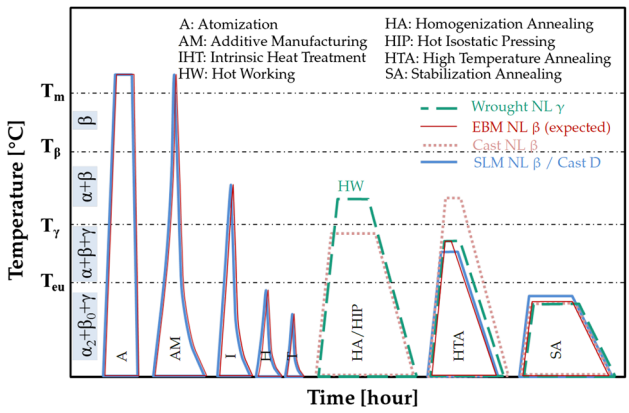

Fig. 2. Process-variant thermal history of various conventional and AM processes with data from Refs. 38, 39, and 40.

resistance with an increasing Al content; the thermodynamic stability still ends several hundred degrees below the melting temperature range.[1,35]

Hence, there are certain constraints towards the process-reliable manufacturing of γ-TiAl hardware coming from the brittle behavior below BDTT or rather from the favorable processing above, and the corresponding need to avoid oxygen exposure during melting and certain stages of cooling. Considering the rather compact dimensions of cold-gas propulsion systems,[15] additive manufacturing becomes a competitive production approach.[36] Besides the well-known freedom of design aspect,[37] there is a great potential of targeted microstructural adaptation coming from the specific thermal boundery conditions. This aspect shall be emphazised using the example of electron beam melting and hybrid laser metal deposition with powder.

ADDITIVE MANUFACTURING

Thermal Characteristics

The thermal profile for additive manufacturing (AM) is significantly different from conventional processing. Furthermore, in the field of AM, there are various processes, each having specific thermal characteristics. However, similar post-heat treatment steps are frequently applied to both conventional and AM processes, such as two- or three-step annealing treatment and/or hot isostatic pressing (Fig. 2).

In the present paper, the focus is on the thermal characteristic of electron beam melting (EBM) and hybrid laser metal deposition (LMD) addressing intrinsic heat treatment and the general boundary conditions of solidification.

Electron Beam Melting

EBM is an additive manufacturing powder-based process. The powder bed is sintered and selectively melted layer-by-layer with an electron beam in a high vacuum atmosphere. The electron beam has a deflection speed up to 8000 m/s and allows the preheating and/or post-heating of the top of the powder bed above the BDTT. In this way, a homogeneous lateral temperature distribution can be achieved. On the other hand, there is an increasing vertical temperature gradient with an increase in build-up height (see Fig. 3a and b).[41] This gradient occurs because of the exclusive heat input via the powder bed surface.

Figure 3a shows nine representative convergent–divergent nozzles, while Fig. 3b shows the corresponding time-temperature diagram from the layer-wise build-up with reference to the build-up height. Considering a melting temperature of 1618°C[42] in the work plane, the intrinsic heat treatment takes

(a)

(b)

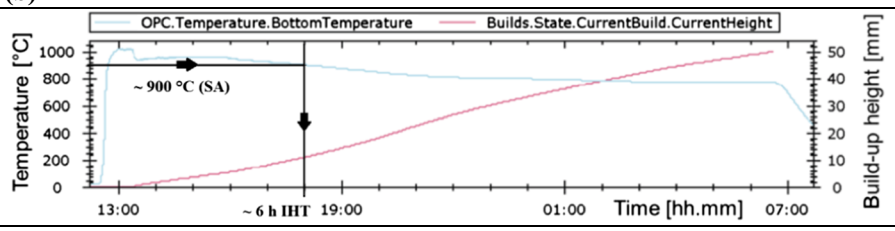

(c)

Process Step	Target surface temperature [°C]	Duration [s]
Pre-heating	1000	13
Melting	Liquidus[1.)]	7[2.)]
Post-heating	1000	20
Raking	No heat input during	10

[1.)] Depending on the nominal composition of the alloy
[2.)] Depending on the geometry of the part or component (melt area)

Fig. 3. (a) Thruster nozzle demonstrators 50 mm height. (b) Build-up height related T-t sequence and (c) representative process cycles for a single powder layer of Ti-43.5Al-4Nb-1Mo-0.1B and a layer thickness of 100 μm.

place passing the temperature fields of high-temperature annealing in the $\beta + \alpha + \gamma$ phase field, and high-temperature annealing and stabilization annealing in the $\beta_0 + \alpha_2 + \gamma$ phase field (Figs. 2 and 3b). The latter is associated with a temperature of approximately 900°C. Looking at a representative process cycle for one layer of Ti-43.5Al-4Nb-1Mo-0.1B (at.%) with a layer thickness of 100 μm (Fig. 3-c), and assuming an insignificant temperature drop during the deposition of the following powder layer, the rake step, the heat input accumulates to approximately 80 min intrinsic heat treatment per centimeter build-up above 900°C.

Seifi et al. stated that the rather higher and complex thermal gradient causes inhomogeneity in the microstructure,[32] which corresponds with results from this investigation. Looking at the top face of the thruster nozzle (see Fig. 4a), a rather coarse α_2-phase (gray, Ti_3Al, hexagonal ordered $D0_{19}$) can be seen. The α_2-phase is surrounded by β_o-phase (light gray Ti(Al), simply cubic-ordered B2). In addition, there is a lamellar γ-phase (dark gray) which is precipitated in the α_2-phase (TiAl, tetragonal $L1_0$). On the other hand, looking at the bottom face of the thruster nozzles (Fig. 4b), there is a rather fine acicular α_2-phase (light gray) distributed with different orientations and surrounded by the β_o-phase (white). The γ-phase (dark gray) is precipitated as a lamellar structure within the α_2-phase and as globular grains in addition to the α_2-phase. These findings are in accordance with results from the literature,[43,44] and correspond with the findings of Clemens et al. describing the development of the phase fraction during a two-step heat treatment.[45] The first step is high-temperature annealing (1230°C for 1 h) in the $\alpha + \beta$ region (see Figs. 1, 4), while the second step is stabilization-annealing (900°C for 6 h) in the $\beta_0 + \alpha_2 + \gamma$ region. Here, the fine gamma lamellae dissolve to alpha thin lamellae forming thick lamellae or the globular γ-phase (Fig. 4c).

Hybrid Laser Metal Deposition

LMD with powder is a generative laser procedure in which material is applied to existing parts or components in layers. The laser generates a localized melt pool on the existing surface and in which powdery filler material is continuously delivered through a nozzle. The powder melts and bonds with the base material. In order to overcome the BDTT, LMD with powder was extended by an additional energy source (inductive heating) (Fig. 5). With the interaction of both the global heat input from the inductive heating, with a pre-heating temperature of 960°C,[12] and the localized heat input of the laser beam (hybrid approach), the temperature can be securely keep above the BDTT. This set-up is integrated in a protective gas chamber which enables the reduction of residual oxygen to less than 100 ppm.[41]

Nevertheless, looking at the melt pool (Fig. 5a), there is a significant difference since there is a liquid/gaseous interface (powder and carrier gas and shielding gas). In consequence, there is a higher cooling rate since heat conduction, convection and radiation become effective as transport mechanisms of thermal energy.[46] Hence, there is a comparatively high-temperature gradient but a rather low solidification rate,[30] because of the permanent heat input with no interruption for the deposition of the powdery filler material (Fig. 5a), and the by orders of magnitude lower feed rate of the energy source if compared to the electron beam. However, the influence of the cooling rate on the microstructural content was studied in situ by Erdely et al.[46] for a multi-phase intermetallic β-stabilized TiAl alloy. The effect of the higher cooling rate can also be observed when looking at the interface between the

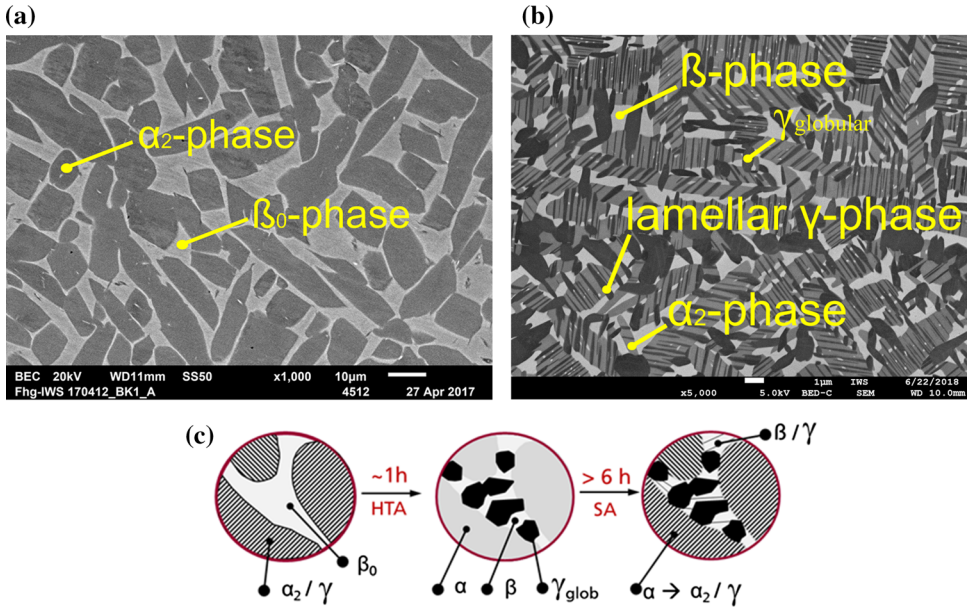

Fig. 4. (a) BEC images of metallographic sections from the top face of the thruster nozzle. (b) Metallographic section of a layer located at the start plate exposed to ~ 18 h in situ heat treatment. (c) Development of the microstructural content during the two-step HT according to Clemens et al.[45]

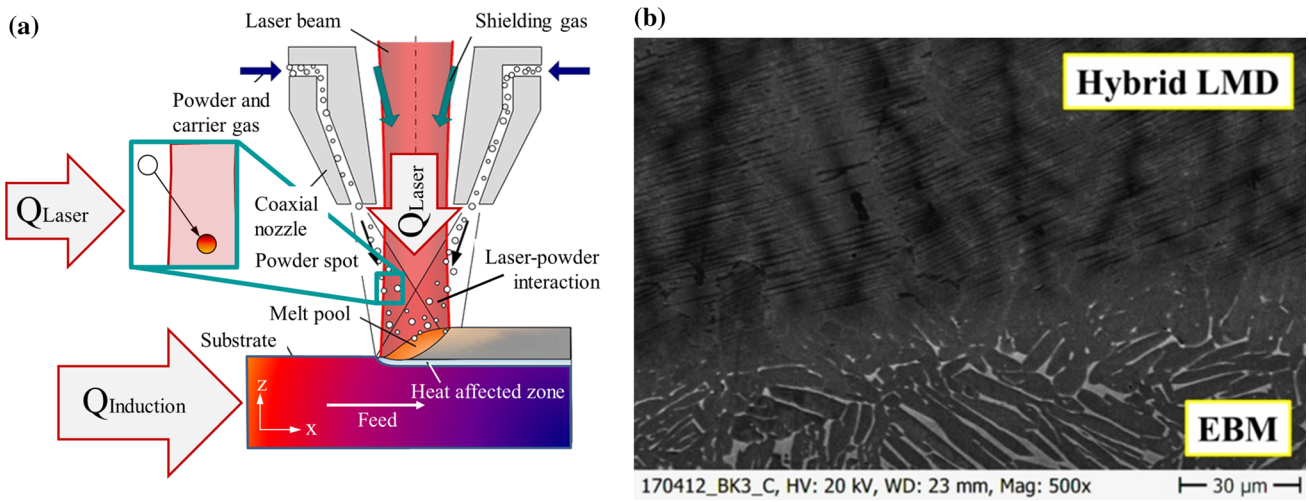

Fig. 5. (a) LMD with powder process zone with additional energy input via inductive heating.[29] (b) EBM-manufactured Ti-43.3Al-4.3Nb-1.2Mo-0.1B (at.%) alloy nozzle after radial laser metal deposition with the same type of powder showing the transition zone between the first laser metal deposition layer (top) and the via electron beam melting manufactured substrate (bottom).

substrate material, manufactured via EBM, and the adjacent layer, manufactured via hybrid LMD with powder. The microstructural content of the substrate corresponds with the findings from the top face of the thruster nozzle (cf. Fig. 3a). The LMD section shows α_2/γ lamellae (light gray), γ-TiAl (dark gray) and just minor content of β_o-TiAl (white phase). Furthermore, the dendritic growth indicates the aforementioned thermal boundary conditions of solidification (see Fig. 5b). With hybrid laser metal deposition, the cooling rate can also be further adjusted by the mutual adaption of the pre-heating temperature, the laser power and the applied process gases (Fig. 5a). In Fig. 6, it can be seen that the microstructural parameters of the lamellar colony size and the lamellar spacing, which are a function of the cooling rate, vary considerably. Deviating from EBM, there is only a short high-temperature annealing in the $\beta + \alpha + \gamma$ phase field related to the limited heat-affected zone of the laser (Fig. 5a). In consequence, there are different mechanical properties to be expected, since ductility and creep properties vary significantly depending on the microstructure.[1]

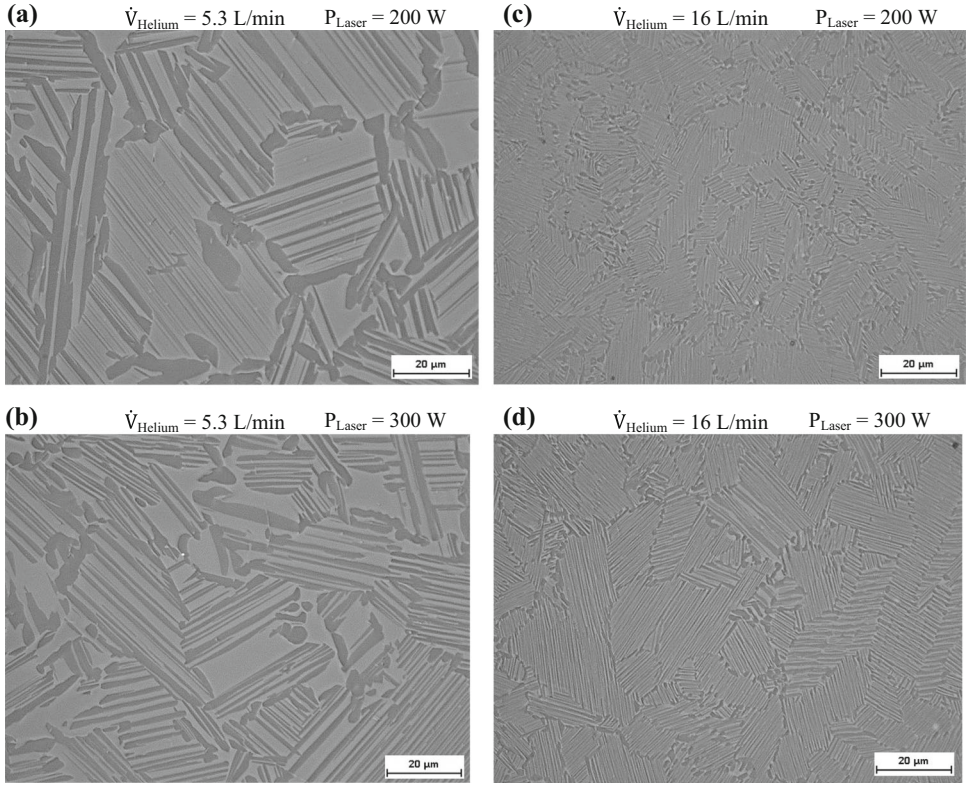

Fig. 6. (a–d) Microstructure overview of selected micrographs produced using different inert gas flow rates and laser powers; the microstructure with minimized inert gas volume flow has a clearly coarse lamellar microstructure, dark γ-phase, light α_2 phase.

CONCLUSION

- High-performance multi-phase materials can be processed within constricted process windows with EBM and hybrid LMD,
- Intrinsic heat treatment in EBM can be related to conventional thermal post-processing in terms of a short high-temperature annealing and several hours of stabilization annealing,
- In hybrid LMD with powder-solidified dendritic with process parameter-dependent lamellar microstructure, the intrinsic heat treatment is related to a short high-temperature annealing,
- The microstructural parameters of the lamellar colony size and the lamellar spacing can be influenced by the adjustment of the pre-heating temperature, laser power and process gas flow,
- The adjustment of the microstructure can provide an additional degree of freedom when considered in the design phase of a part or component in terms of microstructural tailoring, but this need to be further investigated in detail.

REFERENCES

1. H. Clemens and S. Mayer, *Adv. Eng. Mater.* 15, 191 (2013).
2. M. Wolf and M. Vollmuth, *Titanium Aluminide—MTU Aero Engines Develops New Turbine Blade Material: Ceramic-Metal Materials—Lightweight, Creep- and Heat-Resistant First Application in the Geared Turbofan Powering the Airbus A320neo* (Munich, 2017).
3. B.P. Bewlay, M. Weimer, T. Kelly, A. Suzuki, and P.R. Subramanian, *MRS Proc.* 1516, 128 (2013).
4. H. Clemens and W. Smarsly, *AMR* 278, 551 (2011).
5. M. Ivanov, G. Markelov, A. Ketsdever, and D. Wadsworth. (ed), *37th Aerospace Sciences Meeting and Exhibit: Numerical Study of Cold Gas Micronozzle Flows* (1999–1999).
6. A. Anis, *Remote Sensing—Advanced Techniques and Platforms*, ed. B. Escalante (InTech: Rijeka, 2012).
7. M.R. Reid, D.B. Scharfe, F.A.M. Saleem, and R.N. Webb, *J. Propuls. Power* 29, 1488 (2013).
8. A.R. Tummala and A. Dutta, *Aerospace* 4, 58 (2017).
9. M. Gilpin, D. Scharfe, M. Young, and A. Pancotti, in *47th AIAA/ASME/SAE/ASEE Joint Propulsion Conference & Exhibit* (American Institute of Aeronautics and Astronautics, 2011).
10. B. Zhao, J. Sun, J. Sheng Wu, and Z. Xin Yuan, *Scr. Mater.* 46, 581 (2002).
11. *47th AIAA/ASME/SAE/ASEE Joint Propulsion Conference & Exhibit* (American Institute of Aeronautics and Astronautics, 2011).
12. A. Seidel, T. Maiwald, T. Finaske, S. Polenz, S. Saha, M. Riede, J. Moritz, J. Kaspar, F. Brueckner, E. Lopez, C. Leyens, and A. Marquardt, in MS&T, vol. 18, p. 13.
13. R. Ranjan, S.K. Chou, F. Riaz, and K. Karthikeyan, *Energy Proc.* 143, 754 (2017).
14. R.L. Kelley and D. Jarkey, in *AIAA SPACE 2015 Conference and Exposition*.
15. Y.-W. Kim, *JOM* 46, 30 (1994).
16. E. Schwaighofer, M. Schloffer, T. Schmoelzer, S. Mayer, J. Lindemann, V. Guether, J. Klose, and H. Clemens, *PM* 49, 124 (2012).
17. H. Clemens, B. Boeck, W. Wallgram, T. Schmoelzer, L.M. Droessler, G.A. Zickler, H. Leitner, and A. Otto, *MRS Proc.* 1128, 183 (2008).

18. M. Schloffer, T. Schmoelzer, S. Mayer, E. Schwaighofer, G. Hawranek, F.-P. Schimansky, F. Pyczak, and H. Clemens, *PM* 48, 594 (2011).
19. U. Hecht, V. Witusiewicz, A. Drevermann, and J. Zollinger, *Intermetallics* 16, 969 (2008).
20. W.G. Burgers, *Physica* 1, 561 (1934).
21. F. Appel, J.D.H. Paul, and M. Oehring, *Gamma Titanium Aluminide Alloys: Science and Technology: Science and Technology* (Weinheim: Wiley, 2012).
22. R.I. Jaffee and N.E. Promisel, *The Science, Technology and Application of Titanium: Proceedings of an International Conference Organized by the Institute of Metals, the Metallurgical Society of Aime, and the American Society for Metals in Association with the Japan Institute of Metals and the Academy of Sciences, U.S.S.R., and Held at th: Proceedings of an International Conference Organized by the Institute of Metals, the Metallurgical Society of Aime, and the American Society for Metals in Association with the Japan Institute of Metals and the Academy of Sciences, U.S.S.R., and Held at th* (Elsevier Science, Kent, 2014).
23. M. Peters and C. Leyens, *Titan und Titanlegierungen* (Weinheim: Wiley-VCH, 2002).
24. R.T. Zheng, Y.G. Zhang, and C.Q. Chen, *J. Mater. Sci.* 39, 1721 (2004).
25. K.S. Chan and Y.-W. Kim, *Metall. Mater. Trans. A* 23, 1663 (1992).
26. H. Inui, M.H. Oh, A. Nakamura, and M. Yamaguchi, *Acta Metall. Mater.* 40, 3095 (1992).
27. J. Arata, K.S. Kumar, W.A. Curtin, and A. Needleman, *Int. J. Fract.* 111, 163 (2001).
28. F. Brückner, D. Lepski, and E. Beyer, *J. Therm. Spray Technol.* 16, 355 (2007).
29. A. Seidel, T. Finaske, A. Straubel, H. Wendrock, T. Maiwald, M. Riede, E. Lopez, F. Brueckner, and C. Leyens, *Metall. Mater. Trans. A* 49, 3812 (2018).
30. J. Wang, K. Yang, N. Liu, L. Jia, G.Y. Yang, and H.P. Tang, *JOM* 69, 2751 (2017).
31. M. Seifi, I. Ghamarian, P. Samimi, U. Ackelid, P. Collins, and J. Lewandowski, *Microstructure and Mechanical Properties of Ti-48Al-2Cr-2Nb Manufactured Via Electron Beam Melting* (2016).
32. C. Körner, *Int. Mater. Rev.* 61, 361 (2016).
33. A. Donchev and M. Schütze, *Minimization of the Oxygen Embrittlement of Ti-Alloys* (Theodor-Heuss-Allee 25, 60486 Frankfurt am Main, 2010).
34. J.L. Smialek, J.A. Nesbitt, W.J. Brindley, M.P. Brady, J. Doychak, R.M. Dickerson, and D.R. Hull, *MRS Proc.* 364, 207 (1994).
35. E. Glenn Lightsey, T. Stevenson, and M. Sorgenfrei, *Proc. IEEE* 106, 379 (2018).
36. C. Klahn, B. Leutenecker, and M. Meboldt, *Proc. CIRP* 21, 138 (2014).
37. L. Löber, F.P. Schimansky, U. Kühn, F. Pyczak, and J. Eckert, *J. Mater. Process. Technol.* 214, 1852 (2014).
38. S. Mayer, P. Erdely, F.D. Fischer, D. Holec, M. Kastenhuber, T. Klein, and H. Clemens, *Adv. Eng. Mater.* 19, 1600735 (2017).
39. E. Schwaighofer, H. Clemens, S. Mayer, J. Lindemann, J. Klose, W. Smarsly, and V. Güther, *Intermetallics* 44, 128 (2014).
40. A. Seidel, A. Straubel, T. Finaske, T. Maiwald, S. Polenz, M. Albert, J. Näsström, A. Marquardt, M. Riede, E. Lopez, F. Brueckner, E. Beyer, and C. Leyens, *J. Laser Appl.* 30, 32301 (2018).
41. N.A. Belov and I.S. Chupakhin, *Met. Sci. Heat Treat.* 55, 486 (2014).
42. H. Voggenreiter and M. Bartsch (eds), *Selektives Laserschmelzen von konventionellen und intermetallischen Titanlegierungen—Eigenschaften und Optimierung* (2013).
43. H. Tang, S. Lu, W. Jia, G. Yang, and M. Qian, *Int. J. Powder Metall.* 57, 251 (2014).
44. O. Paris, R.T. Lechner, and H. Kirchberger, eds., *6th European Winter School on Neutron and Synchrotron Radiation Planneralm: Materials for Aircraft Engines* (Leoben: Montanuniversität Leoben, 2011).
45. S.M. Thompson, L. Bian, N. Shamsaei, and A. Yadollahi, *Addit. Manuf.* 8, 36 (2015).
46. P. Erdely, R. Werner, E. Schwaighofer, H. Clemens, and S. Mayer, *Intermetallics* 57, 17 (2015).